ELSEVIER

Comput. Methods Appl. Mech. Engrg. 191 (2002) 2979–2995

Computer methods in applied mechanics and engineering

www.elsevier.com/locate/cma

# Development of a sixth-order two-dimensional convection–diffusion scheme via Cole–Hopf transformation

Tony W.H. Sheu *, C.F. Chen, L.W. Hsieh

*Department of Engineering Science and Ocean Engineering, College of Engineering, National Taiwan University, 73 Chou-Shan Road, Taipei, Taiwan, ROC*

Received 6 August 2001; received in revised form 17 December 2001

**Abstract**

In this paper, we develop a two-dimensional finite-difference scheme for solving the time-dependent convection–diffusion equation. The numerical method exploits Cole–Hopf equation to transform the nonlinear scalar transport equation into the linear heat conduction equation. Within the semi-discretization context, the time derivative term in the transformed parabolic equation is approximated by a second-order accurate time-stepping scheme, resulting in an inhomogeneous Helmholtz equation. We apply the alternating direction implicit scheme of Polezhaev to solve the Helmholtz equation. As the key to success in the present simulation, we develop a Helmholtz scheme with sixth-order spatial accuracy. As is standard practice, we validated the code against test problems which were amenable to exact solutions. Results show excellent agreement for the one-dimensional test problems and good agreement with the analytical solution for the two-dimensional problem. 

*Keywords:* Two dimensional; Convection–diffusion equation; Cole–Hopf equation; Nonlinear; Inhomogeneous Helmholtz equation

## 1. Introduction

In this paper, we develop a numerical method for solving the practically important time-dependent nonlinear convection–diffusion scalar transport equation. Besides its broad range of application in areas of fluid dynamics and heat transfer, this equation is also academically important since it is regarded as the simplest prototype equation for modeling most of the transport phenomena. Its practical significance and theoretical importance make numerical prediction of this model equation worthwhile and motivate the present study. We restrict our attention to the two-dimensional case in the $x$–$y$ plane.

A reliable transport scheme must have the ability to suppress convective instabilities, which are particularly severe when convective terms dominate diffusive terms in multidimensions [1]. One way of circumventing this difficulty is to apply the Cole–Hopf transformation [2,3] to map the nonlinear

* Corresponding author. Fax: +886-2-2392-9885.
*E-mail address:* sheu@sccs.na.ntu.edu.tw (T.W.H. Sheu).

0045-7825/02/$ - see front matter 
PII: S0045-7825(02)00220-7

convection–diffusion equation to a transient heat conduction equation. The need to discretize convective terms is, thus, avoided. In this context, how to construct a scheme for the resulting much simple linear parabolic equation becomes the main theme of the present study.

When solving the reduced wave (or Helmholtz) equation by the standard Galerkin finite-element or the second-order centered finite-difference method, the phase accuracy deteriorates rapidly with the increasing wave number [4]. This resolution problem arises from the use of piecewise polynomial shape functions to approximate the highly oscillatory character of the propagating solutions. To obtain an acceptable level of accuracy, more than 10 elements (or stencil points) per wavelength are required [5]. Refining the mesh is considered a natural choice to satisfy this requirement. However, the analysis may become prohibitively expensive and is computationally infeasible for solving the reduced wave equation with large wave numbers. Other methodologies are needed to counteract the pathologies exhibited by the conventional methods. Toward this direction, several approaches designed to improve the numerical phase accuracy have been emerged in the past two decades. Goldstein [6] approximated the Helmholtz solution within each element by the sum of exponentials. The success of extending this approach to the two-dimensional problem has been limited. Park and Jensen [7] conducted discrete Fourier analysis to derive wave number dependent modifications to the Galerkin matrix equations. The dispersion error over a specified frequency-wave number window is minimized. Harari and Hughes [8] appended residuals of the Euler–Lagrange equations in the least-squares form to the standard Galerkin formulation. By virtue of the dispersion analysis, the derived local mesh parameter enables us to obtain an accurate solution with relatively coarse meshes. More recently, Thompson and Pinsky [9] employed the Fourier analysis and successfully derived the optimal Galerkin least-squares parameter for the two-dimensional Helmholtz equation. Based on the pioneer work of Hughes [10], Oberai and Pinsky [11] proposed a multiscale finite element method for the Helmholtz equation to resolve the resolution problem.

In the finite-difference context, there are few high-order schemes for the Helmholtz equation [12]. Besides the well-known five-point finite-difference scheme [13], the nine-point fourth-order scheme of Rosser [14], optimal scheme of Yu [12], and finite analytic scheme of Yu [15] are often referred to. Since compact schemes have been widely applied to solve other differential equations, we will develop in this paper a compact high-resolution Helmholtz scheme. Our goal of solving the transformed model equation is to obtain solutions with higher accuracy at less computational cost.

The rest of this paper is organized as follows. Section 2 presents the working equation and the employed alternating direction implicit (ADI) two-step solution algorithm. In Section 3, we transform the convection–diffusion nonlinear equation into the Helmholtz equation. This is followed by presentation of the Helmholtz scheme in two dimensions using the ADI scheme of Polezhaev [16]. Our emphasis is on the development of a highly accurate Helmholtz scheme on the most compact stencil points. Section 4 is devoted to modified equation analysis of the proposed flux discretization scheme. Section 5 presents numerical results to show the validity of the method. In Section 6, we give concluding remarks.

## 2. Working equation and solution algorithm

We consider in this paper the following nonlinear equation for $u$ in the two-dimensional domain $\Omega$:

$$\frac{\partial u}{\partial t} + u\frac{\partial u}{\partial x} + v\frac{\partial u}{\partial y} - k\left(\frac{\partial^2 u}{\partial x^2} + \frac{\partial^2 u}{\partial y^2}\right) = 0. \tag{2.1}$$

In the above equation, $u$ and $v$ represent velocity components along the $x$ and $y$ directions, respectively, and $k$ denotes the diffusion coefficient. For purposes of illustration, we assume that all physical properties are

uniform throughout the domain of flow. The above parabolic equation will be solved subject to the initial condition as well as the boundary condition.

For purposes of computational efficiency, we calculate $u$ via the following ADI scheme of Polezhaev [16]:

$$\left[\frac{\partial u}{\partial t}+u\frac{\partial u}{\partial x}-k\frac{\partial^2 u}{\partial x^2}\right]^{m+1}=\left[-v\frac{\partial u}{\partial y}+k\frac{\partial^2 u}{\partial y^2}\right]^{m}, \tag{2.2}$$

$$\left[\frac{\partial u}{\partial t}+v\frac{\partial u}{\partial y}-k\frac{\partial^2 u}{\partial y^2}\right]^{m+2}=\left[-u\frac{\partial u}{\partial x}+k\frac{\partial^2 u}{\partial x^2}\right]^{m+1}. \tag{2.3}$$

In the above, the superscripts $m$ and $m+1$ denote two consecutive iteration counters. Within each time step, the calculation proceeds alternatively using the most updated $u$ in the calculation of derivative terms shown in the right-hand side of Eqs. (2.2) and (2.3). The above iterative procedures continue until the user's specified tolerance is reached. As Eqs. (2.2) and (2.3) reveal, the task of integrating forward in time the two-dimensional convection–diffusion equation (2.1) involves deriving transport schemes for solving nonlinear equation and linear one-dimensional convection–diffusion equations (2.2) and (2.3), respectively.

Amongst the possible ways to rectify numerical instabilities stemming from convective terms in Eq. (2.2), we choose to get rid of the nonlinear term by employing the Cole–Hopf transformation given below [2,3]:

$$u=-2k\frac{\partial(\ln\phi)}{\partial x}, \tag{2.4}$$

or

$$u=\frac{-2k}{\phi}\frac{\partial\phi}{\partial x}. \tag{2.5}$$

In this context, Eq. (2.2) is rewritten in terms of the newly introduced scalar $\phi$ by applying Eq. (2.5) to derive $u_t$, $u_x$ and $u_{xx}$. This is followed by substituting them into Eq. (2.2) to derive an inhomogeneous heat conduction equation for $\phi$ as follows:

$$\frac{\partial\phi}{\partial t}=k\frac{\partial^2\phi}{\partial x^2}+\left[\int_0^x\frac{F(\xi)}{-2k}\,\mathrm{d}\xi\right]\phi, \tag{2.6}$$

where

$$F\equiv\left[-v\frac{\partial u}{\partial y}+k\frac{\partial^2 u}{\partial y^2}\right]^{m}. \tag{2.7}$$

The derivation of Eqs. (2.6) and (2.7) is detailed in Appendix A.

Besides transforming the working equation, both boundary and initial conditions need to be transformed. Given the boundary conditions of $u$ as $u(x_1,t)$ and $u(x_2,t)$ one can easily derive the boundary conditions of the Robin type for $\phi$ by means of the Cole–Hopf transformation given in Eq. (2.5):

$$u(x_1,t)\phi+2k\frac{\partial\phi}{\partial x}=0, \tag{2.8}$$

$$u(x_2,t)\phi+2k\frac{\partial\phi}{\partial x}=0. \tag{2.9}$$

The initial condition $\phi(x,t=0)$ can be similarly derived by integrating Eq. (2.5) with respect to $x$ to yield

$$\phi(x,0)=\phi_0(x)=C_0\exp\left[-\frac{1}{2k}\int_0^x u_0(\xi)\,\mathrm{d}\xi\right]. \tag{2.10}$$

If we substitute $\phi(x,t)$ into Eq. (2.5), $C_0$ will be cancelled out and, thus, can be arbitrarily chosen. In the present study, we set $C_0 = 1$.

Discretization of Eq. (2.6) begins with approximating $\partial\phi/\partial t$ using the following second-order time-stepping scheme:

$$\frac{\partial\phi^{n+1}}{\partial t} = \frac{3\phi^{n+1} - 4\phi^n + \phi^{n-1}}{2\Delta t}, \tag{2.11}$$

Application of $(\partial\phi/\partial t) = k(\partial^2\phi/\partial x^2) + [\int_0^x (F(\xi)/-2k)\,\mathrm{d}\xi]\phi$ enables us to obtain the following inhomogeneous Helmholtz equation from Eq. (2.6):

$$\frac{\partial^2\phi^{n+1}}{\partial x^2} + \frac{1}{k}\left[\int_0^x \frac{F(\xi)}{-2k}\,\mathrm{d}\xi - \frac{3}{2\Delta t}\right]\phi^{n+1} = f, \tag{2.12}$$

where

$$f = \frac{-4\phi^n + \phi^{n-1}}{2k\Delta t}. \tag{2.13}$$

When calculating the first derivative terms in the source term, more modal points at the upwind side are considered. As an illustrative example, we consider that $\bar{a} > 0$ in the approximation of $\bar{a}(\partial u/\partial x)$. The value $h(\partial u/\partial x)\,(\equiv H)$, where $h$ denotes the grid size, at $j$ is computed implicitly from

$$\alpha_0 H_{j+1} + \beta_0 H_j + \gamma_0 H_{j-1} = b(u_{j+1} - u_j) + c(u_j - u_{j-1}) + d(u_{j-1} - u_{j-2}). \tag{2.14}$$

Here, $\alpha_0$, $\beta_0$, $\gamma_0$, $b$, $c$ and $d$ are determined as 21, 36, 3, 50, 8 and 2 according to modified equation analysis.

Throughout this paper, the second derivative terms can be similarly approximated. Take $\partial^2\phi/\partial x^2$ at a node $j$ as an example; $G_j \equiv h^2(\partial^2\phi/\partial x^2)|_j$ is implicitly calculated from the following equation:

$$\bar{\alpha}_0 G_{j+1} + \bar{\beta}_0 G_j + \bar{\gamma}_0 G_{j-1} = \bar{a}^*\phi_{j+2} + \bar{b}^*\phi_{j+1} + \bar{c}^*\phi_j + \bar{d}^*\phi_{j-1} + \bar{e}^*\phi_{j-2}. \tag{2.15}$$

By expanding $G_{j\pm1}$ with respect to $G_j$ and $\phi_{j\pm1}$, $\phi_{j\pm2}$ with respect to $\phi_j$ in Taylor series and then substituting them into the expression for $G_j$, we are led to have $(\bar{\alpha}_0, \bar{\beta}_0, \bar{\gamma}_0, \bar{a}^*, \bar{b}^*, \bar{c}^*, \bar{d}^*, \bar{e}^*) = (1, \frac{11}{2}, 1, \frac{3}{8}, 6, -\frac{51}{4}, 6, \frac{3}{8})$ from the resulting algebraic equation.

## 3. Numerical model

As alluded to earlier, the key to success in solving Eq. (2.1) lies in the scheme developed for solving the one-dimensional model equations (2.2) and (2.3). Due to space limitation, we will not detail the linear convection–diffusion scheme for solving Eq. (2.3) (see [17] for details). In this study, we confine ourselves to the derivation of finite-difference scheme for the following Helmholtz equation:

$$\frac{\partial^2\bar{u}}{\partial x^2} + \bar{k}^2\bar{u} = \overline{F}. \tag{3.1}$$

In the above, the wave number $\bar{k}$ may vary with $x$. By differentiating Eq. (3.1) twice with respect to $x$, one obtains

$$\frac{\partial^4\bar{u}}{\partial x^4} = -\bar{k}^2\frac{\partial^2\bar{u}}{\partial x^2} - \left(4\bar{k}\frac{\partial\bar{k}}{\partial x}\right)\frac{\partial\bar{u}}{\partial x} - \left[2\left(\frac{\partial\bar{k}}{\partial x}\right)^2 + 2\bar{k}\frac{\partial^2\bar{k}}{\partial x^2}\right]\bar{u} + \frac{\partial^2\overline{F}}{\partial x^2}. \tag{3.2}$$

In this study, we wish to obtain a highly accurate solution using a scheme which involves as few stencil points as possible. To achieve this goal, we introduce two auxiliary variables, $s$ and $q$, given below to represent the second and fourth derivatives of $\bar{u}$:

$$\frac{\partial^2 \bar{u}}{\partial x^2} = s, \tag{3.3}$$

$$\frac{\partial^4 \bar{u}}{\partial x^4} = q. \tag{3.4}$$

The main innovation of the proposed scheme is that we relate nodal values of $s$, $q$ and $\bar{u}$ implicitly by

$$h^4(\gamma_1 q_{j+1} + \gamma_0 q_j + \gamma_{-1} q_{j-1}) + h^2(\beta_1 s_{j+1} + \beta_0 s_j + \beta_{-1} s_{j-1}) = \alpha_1 \bar{u}_{j+1} + \alpha_0 \bar{u}_j + \alpha_{-1} \bar{u}_{j-1}. \tag{3.5}$$

By expanding $q_{j\pm1}$, $s_{j\pm1}$ and $\bar{u}_{j\pm1}$ with respect to $q_j$, $s_j$ and $\bar{u}_j$, respectively, and then substituting them into Eq. (3.5), we are led to derive the following equation:

$$\begin{aligned}
&h^4(\gamma_1+\gamma_0+\gamma_{-1})q_j + h^5(\gamma_1-\gamma_{-1})\frac{\partial q}{\partial x} + \frac{h^6}{2}(\gamma_1+\gamma_{-1})\frac{\partial^2 q}{\partial x^2} + \cdots + h^2(\beta_1+\beta_0+\beta_{-1})s_j \\
&\quad + h^3(\beta_1-\beta_{-1})\frac{\partial s}{\partial x} + \frac{h^4}{2}(\beta_1+\beta_{-1})\frac{\partial^2 s}{\partial x^2} + \frac{h^5}{6}(\beta_1-\beta_{-1})\frac{\partial^3 s}{\partial x^3} + \frac{h^6}{24}(\beta_1+\beta_{-1})\frac{\partial^4 s}{\partial x^4} + \cdots \\
&= (\alpha_1+\alpha_0+\alpha_{-1})\bar{u}_j + h(\alpha_1-\alpha_{-1})\frac{\partial \bar{u}}{\partial x} + \frac{h^2}{2}(\alpha_1+\alpha_{-1})\frac{\partial^2 \bar{u}}{\partial x^2} + \frac{h^3}{6}(\alpha_1-\alpha_{-1})\frac{\partial^3 \bar{u}}{\partial x^3} \\
&\quad + \frac{h^4}{24}(\alpha_1+\alpha_{-1})\frac{\partial^4 \bar{u}}{\partial x^4} + \frac{h^5}{120}(\alpha_1-\alpha_{-1})\frac{\partial^5 \bar{u}}{\partial x^5} + \frac{h^6}{720}(\alpha_1-\alpha_{-1})\frac{\partial^6 \bar{u}}{\partial x^6} + \frac{h^7}{7!}(\alpha_1+\alpha_{-1})\frac{\partial^7 \bar{u}}{\partial x^7} \\
&\quad + \frac{h^8}{8!}(\alpha_1-\alpha_{-1})\frac{\partial^8 \bar{u}}{\partial x^8} + \cdots
\end{aligned} \tag{3.6}$$

Based on the definitions of $s_j$ and $q_j$ given in Eqs. (3.3) and (3.4), the following equations result:

$$\begin{aligned}
&\alpha_1+\alpha_0+\alpha_{-1} = 0, \\
&\alpha_1-\alpha_{-1} = 0, \\
&\frac{\alpha_1+\alpha_{-1}}{2} = \beta_1+\beta_0+\beta_{-1}, \\
&\frac{\alpha_1-\alpha_{-1}}{6} = \beta_1-\beta_{-1}, \\
&\frac{\alpha_1+\alpha_{-1}}{24} = \frac{\beta_1+\beta_{-1}}{2} + \gamma_1+\gamma_0+\gamma_{-1}, \\
&\frac{\alpha_1-\alpha_{-1}}{120} = \frac{\beta_1-\beta_{-1}}{6} + \gamma_1-\gamma_{-1}, \\
&\frac{\alpha_1+\alpha_{-1}}{720} = \frac{\beta_1+\beta_{-1}}{24} + \frac{\gamma_1+\gamma_{-1}}{2}.
\end{aligned} \tag{3.7}$$

Setting $\gamma_1 = \gamma_{-1} = 41$, We obtain $\alpha_1 = \alpha_{-1} = -5040$, $\alpha_0 = 10,080$, $\beta_1 = \beta_{-1} = -660$, $\beta_0 = -3720$ and $\gamma_0 = 158$.

The derivation is followed by substituting

$$s = -\bar{k}^2 \bar{u} + \overline{F}, \tag{3.8}$$

$$\begin{aligned}
q &= -\bar{k}^2 s - \left(4\bar{k}\frac{\partial \bar{k}}{\partial x}\right)\frac{\partial \bar{u}}{\partial x} - \left[2\left(\frac{\partial \bar{k}}{\partial x}\right)^2 + 2\bar{k}\frac{\partial^2 \bar{k}}{\partial x^2}\right]\bar{u} + \frac{\partial^2 \overline{F}}{\partial x^2} \\
&= -\left(4\bar{k}\frac{\partial \bar{k}}{\partial x}\right)\frac{\partial \bar{u}}{\partial x} - \left[2\left(\frac{\partial \bar{k}}{\partial x}\right)^2 + 2\bar{k}\frac{\partial^2 \bar{k}}{\partial x^2} - \bar{k}^4\right]\bar{u} - \bar{k}^2\overline{F} + \frac{\partial^2 \overline{F}}{\partial x^2},
\end{aligned} \tag{3.9}$$

into Eq. (3.5) to derive the following three-point stencil equation for Eq. (3.1)

$$\bar{a}_i\bar{u}_{i-1} - \bar{b}_i\bar{u}_i + \bar{c}_i\bar{u}_{i+1} = \bar{f}. \tag{3.10}$$

For brevity, we shall in what follows express coefficients shown above for the constant coefficients case:

$$\bar{a}_i = \bar{c}_i = -5040 - 660h^2\bar{k}^2 - 41h^4\bar{k}^4, \tag{3.11a}$$

$$\bar{b}_i = -10,080 + 3720h^2\bar{k}^2 + 158h^4\bar{k}^4, \tag{3.11b}$$

$$\bar{f} = (-660h^2 - 41h^4\bar{k}^2)(\overline{F}_{i+1} + \overline{F}_{i-1}) + (-3720h^2 - 158h^4\bar{k}^2)\overline{F}_i + 41h^4\left(\frac{\partial^2\overline{F}}{\partial x_{i+1}^2} + \frac{\partial^2\overline{F}}{\partial x_{i-1}^2}\right) + 158h^4\frac{\partial^2\overline{F}}{\partial x_i^2}. \tag{3.11c}$$

Expanding $\bar{u}_{j\pm1}$ in a Taylor series with respect to $\bar{u}_j$ yields the following modified equation [18] for the proposed discretization equation after some algebra:

$$\bar{k}^2\bar{u} + \frac{\partial^2\bar{u}}{\partial x^2} = \frac{-1}{(-5040h^2 - 240h^4\bar{k}^2)}\left[-(420h^4 + 41h^6\bar{k}^2)\left(\bar{k}^2\frac{\partial^2\bar{u}}{\partial x^2} + \frac{\partial^4\bar{u}}{\partial x^4}\right) - \left(14h^6 + \frac{41}{12}h^8\bar{k}^2\right)\left(\bar{k}^2\frac{\partial^4\bar{u}}{\partial x^4} + \frac{\partial^6\bar{u}}{\partial x^6}\right) + \frac{\partial^6\bar{u}}{\partial x^6}\left(\frac{19}{12}h^8\bar{k}^2 - \frac{41}{360}h^{10}\bar{k}^4\right)\right] + \text{HOT}. \tag{3.12}$$

By virtue of $\bar{k}^2(\partial^2\bar{u}/\partial x^2) + \partial^4\bar{u}/\partial x^4 = \partial^2\overline{F}/\partial x^2$ and $\bar{k}^2(\partial^4\bar{u}/\partial x^4) + \partial^6\bar{u}/\partial x^6 = \partial^4\overline{F}/\partial x^4$, the above modified equation can be further simplified as follows provided that $\bar{k}$ is a constant.

$$\bar{k}^2\bar{u} + \frac{\partial^2\bar{u}}{\partial x^2} - \overline{F} = h^6\left(A + Bh^2 + \cdots\right)\frac{\partial^6\bar{u}}{\partial x^6} + \text{HOT}, \tag{3.13}$$

where

$$A = \frac{19\bar{k}^2}{60,480}, \tag{3.14a}$$

$$B = \frac{-477\bar{k}^4}{12,700,800}. \tag{3.14b}$$

Note that the order of accuracy remains as six for the variable wave number case using the three-point stencil scheme. Therefore, we can apply the computationally most effective tri-diagonal Thomas direct solution solver to obtain the solution [19].

## 4. Fundamental study on the proposed transient heat conduction scheme

Having presented the scheme for the Helmholtz equation, we can now proceed to derive the discretized equation for Eq. (2.12). This can be done by simply substituting $\bar{u} = \phi$, $\bar{k}^2 = (1/k)[\int_0^x F(\xi)/(-2k)\,\mathrm{d}\xi - 3/(2\Delta t)]$ and $\overline{F} = f$, defined in Eq. (2.13), into Eq. (3.1). After some algebra, the modified equation for this discretized equation will result as

$$\frac{\partial^2\phi}{\partial x^2} + K^2\phi - f = \mathrm{O}(h^6). \tag{4.1}$$

In the above, we introduced a variable $K^2 = (1/k)[\int_0^x F(\xi)/(-2k)\,\mathrm{d}\xi - 3/(2\,\Delta t)]$ for simplicity. Since any implicit scheme is unconditionally stable, a convergent solution is expected to obtain thanks to the Lax's equivalence theorem [20].

As Eq. (3.11a) shows, the coefficients for $\bar{u}_{j\pm1}$ are unconditionally negative in magnitude. This is not the case for the coefficient $\bar{b}_i$ shown in Eq. (3.11b). Depending on the chosen grid size $h$, the coefficient for $\bar{u}_j$ can be negative or positive. Given a value of $\bar{k}$, we can determine $h$ so that $10,080 - 3720h^2\bar{k}^2 - 158h^4\bar{k}^4 > 0$. If this is the case, coefficients in Eq. (3.10) satisfy the following two properties: (i) $\bar{b}_i > 0$, $\bar{c}_i < 0$ and $\bar{a}_i < 0$; (ii) $|\bar{b}_i| > |\bar{a}_i| + |\bar{c}_i|$. Under these circumstances, the matrix equation for $\bar{a}_i\bar{u}_{i-1} - \bar{b}_i\bar{u}_i + \bar{c}_i\bar{u}_{i+1} = \bar{f}$ is an M-matrix [21,22]. The proposed scheme is, therefore, expected to be able to resolve any sharp profile in the flow.

## 5. Validation study

We will first consider test problems which are amenable to analytical solutions to validate the Helmholtz and the heat conduction schemes. This is followed by solving the nonlinear convection–diffusion equation. Both one- and two-dimensional problems will be investigated.

### 5.1. Validation of the Helmholtz equation

The test problem given below is defined in $0 \leqslant x \leqslant 3\pi/2$:

$$\frac{\partial^2\phi}{\partial x^2} + \phi = 0. \tag{5.1}$$

Subject to the boundary conditions $\phi(0) = 0$ and $\phi(3\pi/2) = 1$, Eq. (5.1) is amenable to analytical solution given by

$$\phi = \sin x. \tag{5.2}$$

For the case with the grid size $h = \pi/10$, it is found from Fig. 1 that the exact solution is reproduced. We also performed computations on continuously refined grids, namely, $h = \pi/10$, $\pi/20$, $\pi/40$, $\pi/60$, and $\pi/80$, and cast the prediction errors in their $L_2$-norms. This was followed by plotting $\log(\mathrm{err}_1/\mathrm{err}_2)$ against $\log(h_1/h_2)$ for the errors $\mathrm{err}_1$ and $\mathrm{err}_2$ computed on two continuously refined grids $h_1$ and $h_2$. As Fig. 2 shows, the rate of convergence is obtained as 6.1 using the proposed scheme.

### 5.2. Validation of the transient heat conduction equation

We then consider the following time-dependent heat conduction equation which is also amenable to exact solution for purposes of validation:

$$\frac{\partial u}{\partial t} = \mu\frac{\partial^2 u}{\partial x^2}. \tag{5.3}$$

Given the initial and boundary conditions, respectively, as

$$u(x,0) = 1 + \sinh x, \tag{5.4a}$$

$$u(0,t) = 1 + \mathrm{e}^{\mu t}\sinh(0), \tag{5.4b}$$

$$u(2\pi,t) = 1 + \mathrm{e}^{\mu t}\sinh(2\pi), \tag{5.4c}$$

the exact solution is derived as [21]

$$u(x,t) = 1 + \mathrm{e}^{\mu t}\sinh(x). \tag{5.5}$$

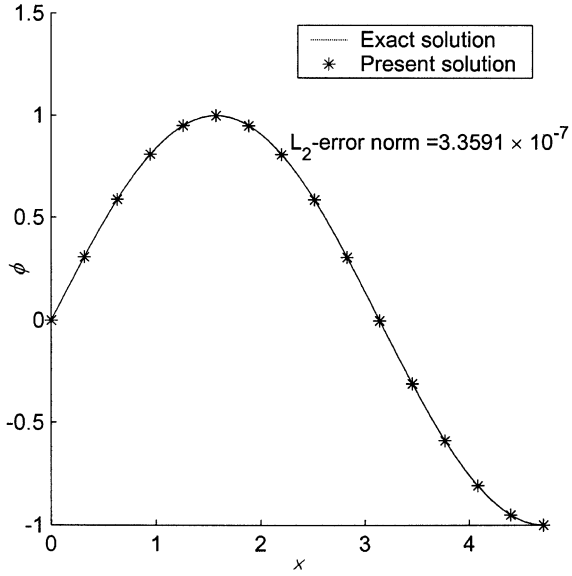


Fig. 1. The comparison of exact and present solutions computed under $\Delta x = \pi/10$ for the test problem given in Section 5.1.

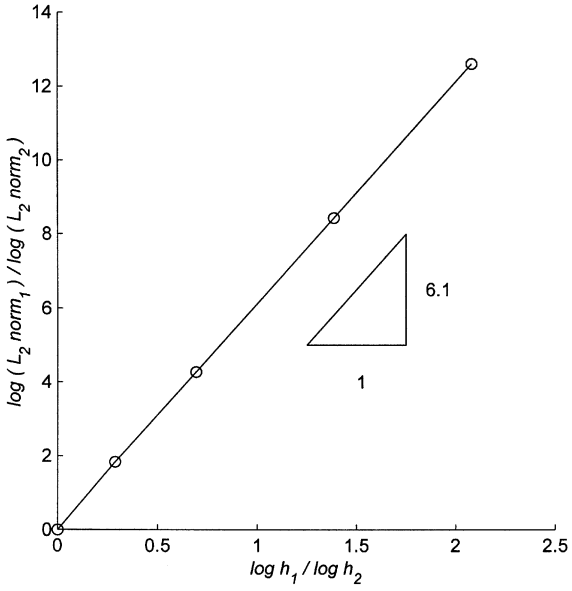


Fig. 2. The computed rate of convergence for the Helmholtz equation given in Section 5.1 using the proposed sixth-order finite-difference scheme.

For the case with $\mu = 1.16$, $\Delta t = 0.05$ and $h = \pi/10$, the results shown in Fig. 3 are found to reproduce the analytical solution given in Eq. (5.5). The integrity of the semi-discretization scheme is, thus, confirmed. As in the analysis of the Helmholtz equation, temporal and spatial rates of convergence were also computed. Computations at $\Delta t = \frac{1}{500}$ were carried out on four continuously refined grids ($h = 0.755, 0.73, 0.707, 0.686$).

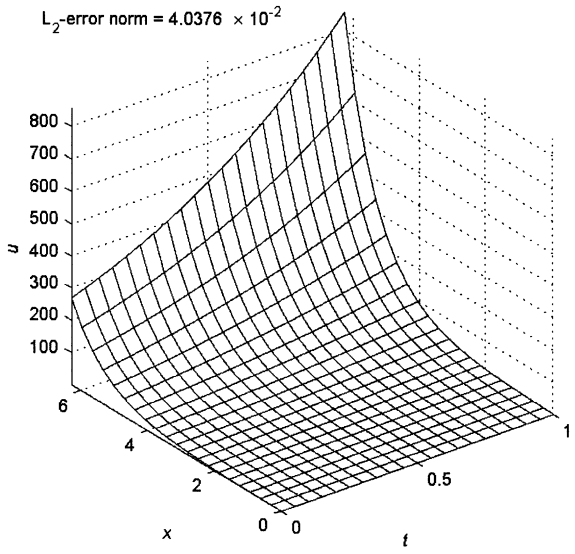


Fig. 3. The finite-difference solutions, computed under $\Delta x = \pi/10$ and $\Delta t = 0.05$, are plotted in $x$–$t$ coordinates for the transient heat conduction equation given in Section 5.2.

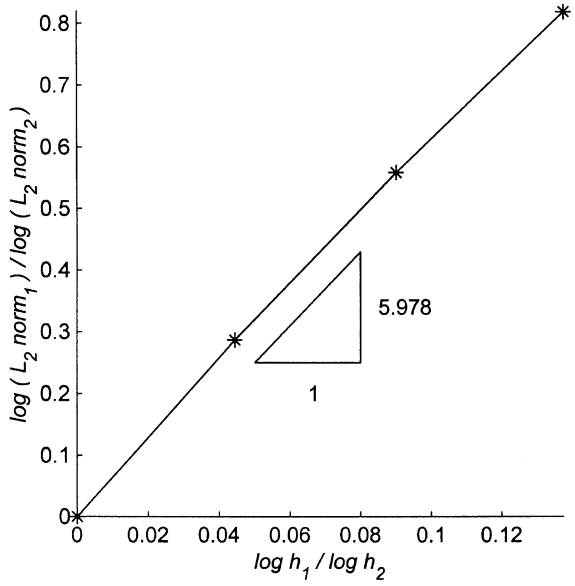


Fig. 4. The computed spatial rate of convergence for the transient heat conduction equation given in Section 5.2 using the proposed semi-discretization finite-difference scheme.

The computed errors, cast in their $L_2$-error norms, are plotted in Fig. 4, from which it is clearly seen that the spatial rate of convergence is obtained as 5.978. Similarly, results obtained at $h = \pi/500$ and four continuously refined time steps ($\Delta t = \frac{1}{100}, \frac{1}{200}, \frac{1}{400}, \frac{1}{800}$) reveal that the $L_2$-error norms decrease with the decreasing time increments. As Fig. 5 shows, the temporal rate of convergence is 1.995.

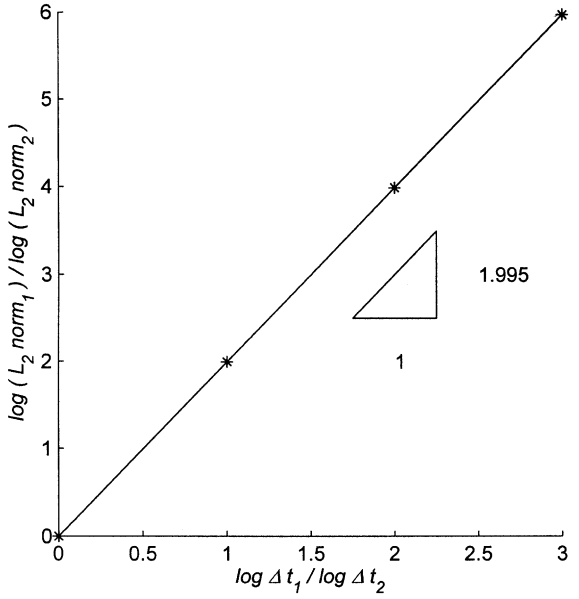


Fig. 5. The computed temporal rate of convergence for the transient heat conduction equation given in Section 5.2 using the proposed semi-discretization finite-difference scheme.

### 5.3. Validation of the convection–diffusion equation

Having validated the scheme for solving the Helmholtz equation and justified the use of the semi-discretization model to solve the time-dependent heat conduction equation, we are to verify the Cole–Hopf mapping used in the analysis of nonlinear convection–diffusion equation. For this purpose, we will consider the following equation:

$$\frac{\partial u}{\partial t} + u\frac{\partial u}{\partial x} = \frac{\partial^2 u}{\partial x^2}. \tag{5.6}$$

The problem under investigation is subject to the following initial and boundary conditions:

$$u(x,0) = \frac{2\pi \sin \pi x + 8\pi \sin 2\pi x}{4 + \cos \pi x + 2\cos 2\pi x}, \tag{5.7a}$$

$$u(0,t) = u(1,t) = 0. \tag{5.7b}$$

For the problem defined in Eqs. (5.6), (5.7a) and (5.7b), its analytical solution can be derived as [2]

$$u(x,t) = \frac{2\pi[\exp(-\pi^2 t)\sin \pi x + 4\exp(-4\pi^2 t)\sin 2\pi x]}{4 + \exp(-\pi^2 t)\cos \pi x + 2\exp(-4\pi^2 t)\cos 2\pi x}. \tag{5.8}$$

The calculations were performed at $h = 0.05$ and $\Delta t = 0.005$. As Fig. 6 shows, solutions plotted at $t = 0.025$, 0.05, 0.1 and 1 agree well with the exact solution given in Eq. (5.8). This confirms that the solutions to nonlinear viscous Burgers equation can be obtained from the proposed methodology.

As alluded to earlier, the proposed scheme is monotonic if the grid size $h$ lies in the range of validity, namely, $10,080 - 3720h^2\bar{k}^2 - 158h^4\bar{k}^4 > 0$. To confirm this, we employ Eq. (5.6), subject to the initial and boundary conditions given below [23]:

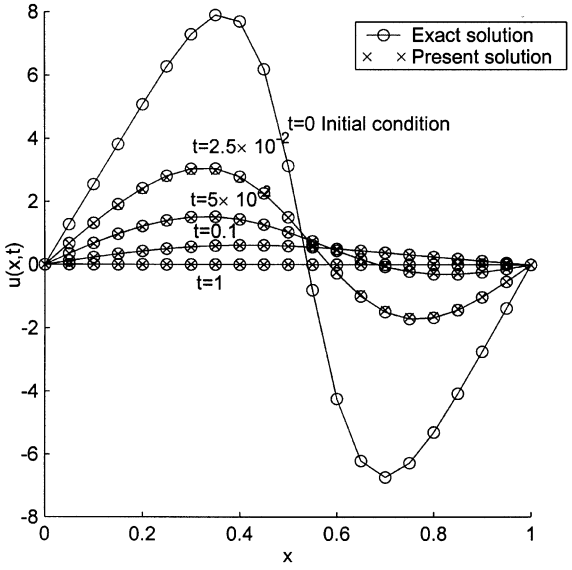


Fig. 6. The comparison of the present and exact solutions at $t = 2.5 \times 10^{-2}$, $5 \times 10^{-2}$, 0.1 and 1 for the test problem given in Eqs. (5.6), (5.7a) and (5.7b).

$$u(x,0) = -2\,\mathrm{sgn}(x), \tag{5.9}$$

and

$$u(-1,t) = 2, \tag{5.10a}$$

$$u(1,t) = -2. \tag{5.10b}$$

The analytical solution is obtained as

$$u(x,t) = 2\frac{G(x,t) - G(-x,t)}{G(x,t) + G(-x,t)}, \tag{5.11}$$

where

$$G(x,t) \equiv \tfrac{1}{2}\mathrm{e}^{t-x}\,\mathrm{erfc}\left(\frac{x-2t}{2\sqrt{t}}\right). \tag{5.12}$$

In the above, $\mathrm{erfc}(z)$ denotes the complementary error function and is defined as $\mathrm{erfc}(z) = 1 - \mathrm{erf}(z)$. This problem is suitable for checking whether the proposed scheme is indeed monotonic. As Fig. 7 shows, sharp profiles were accurately predicted without showing oscillatory solutions in the vicinity of the high-gradient region. The proposed sixth-order scheme is, therefore, classified as a high-resolution capturing scheme.

### 5.4. Validation of the two-dimensional Burgers' equation

Our attention is now drawn to the ADI solution algorithm used to solve the two-dimensional convection–diffusion equation. As previously noted, we need to provide evidence of validity. To this end, we choose to solve the following equation in the rectangle $-10 \leqslant x \leqslant 10$, $0 \leqslant y \leqslant \pi/3$:

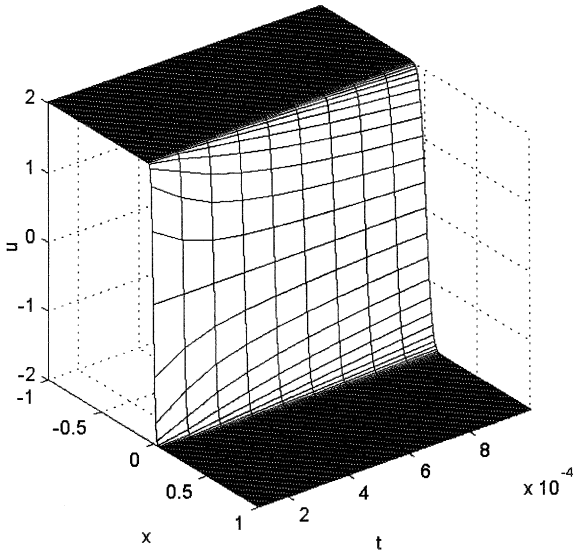


Fig. 7. The computed nonoscillatory solutions for the problem given in Eqs. (5.6), (5.9), (5.10a) and (5.10b).

$$\frac{\partial u}{\partial t}+u\frac{\partial u}{\partial x}+v\frac{\partial u}{\partial y}=\frac{1}{Re}\left(\frac{\partial^2 u}{\partial x^2}+\frac{\partial^2 u}{\partial y^2}\right). \tag{5.13}$$

As an example, $Re$ is set to be 5, and $v$ is assumed to be

$$v=\frac{[\mathrm{e}^{0.5(x-1)}+\mathrm{e}^{-0.5(x-1)}]\sin(0.5y)}{0.005\mathrm{e}(1+x)+5[\mathrm{e}^{0.5(x-1)}+\mathrm{e}^{-0.5(x-1)}]\cos(0.5y)}. \tag{5.14}$$

Subject to the Dirichlet-type boundary condition schematically shown in Fig. 8, the exact steady-state solution to the above nonlinear viscous Burgers equation (5.13) is given by [24]

$$u=\frac{-0.002\mathrm{e}-[\mathrm{e}^{0.5(x-1)}-\mathrm{e}^{-0.5(x-1)}]\cos(0.5y)}{0.005\mathrm{e}(1+x)+5[\mathrm{e}^{0.5(x-1)}+\mathrm{e}^{-0.5(x-1)}]\cos(0.5y)}. \tag{5.15}$$

Following the methodology just described, we first solved the time-dependent heat conduction equation. This was followed by obtaining $u$ from the employed Cole–Hopf transformation equation. In this case, all computed errors were cast in their $L_2$-error norms. We then plotted values of $\log(\mathrm{err}_1/\mathrm{err}_2)$ against $\log(h_1/h_2)$ based on errors $\mathrm{err}_1$ and $\mathrm{err}_2$ computed at two consecutively refined meshes $h=h_1$ and $h=h_2$ With these error norms, the rate of convergence using the proposed scheme was plotted in Fig. 9. Good agreement among the results shown in Fig. 10 and fast convergence to the analytical solution are demonstrated.

Another two-dimensional problem, which is also amenable to exact solution in the square $0\leqslant x, y\leqslant 1$, is under investigation:

$$\frac{\partial u}{\partial t}+u\frac{\partial u}{\partial x}+u\frac{\partial u}{\partial y}=\frac{v}{2}\left(\frac{\partial^2 u}{\partial x^2}+\frac{\partial^2 u}{\partial y^2}\right). \tag{5.16}$$

Subject to the initial and boundary conditions, the exact transient solution is derived as

$$u(x,y,t)=\left(1+\mathrm{e}^{B}\right)^{-1}, \tag{5.17}$$

where

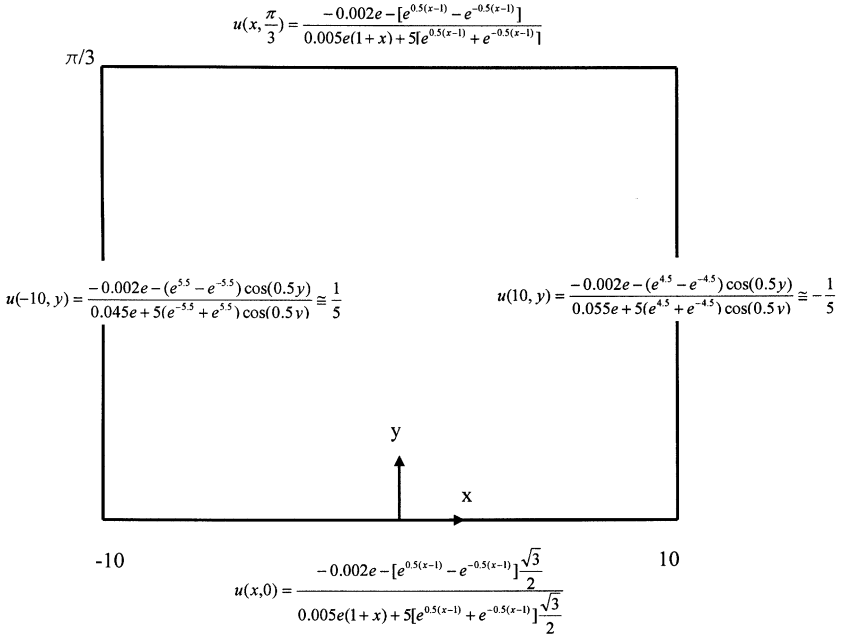


Fig. 8. Schematic of the boundary conditions for the problem given in Eqs. (5.13) and (5.14).

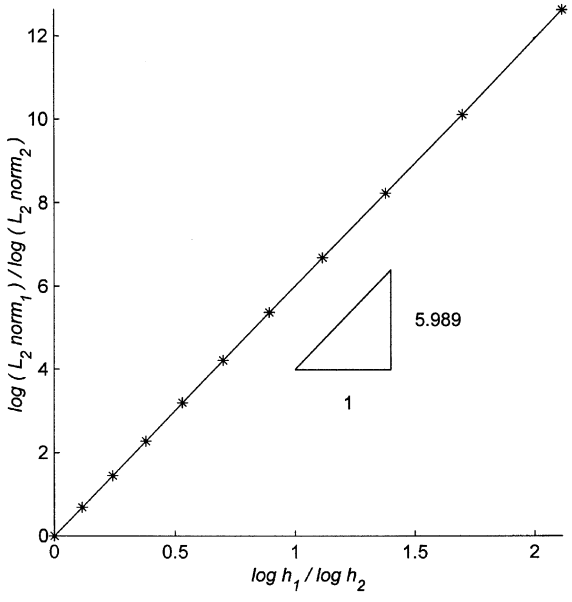


Fig. 9. The computed spatial rate of convergence for the two-dimensional problem given in Eqs. (5.13)–(5.15). This calculation was carried out for grid spacings $(\Delta x, \Delta y) = (20/3, \pi/9), (20/4, \pi/12), (20/5, \pi/15), \ldots, (20/13, \pi/39)$.

$$B \equiv \frac{x+y-t}{v}. \tag{5.18}$$

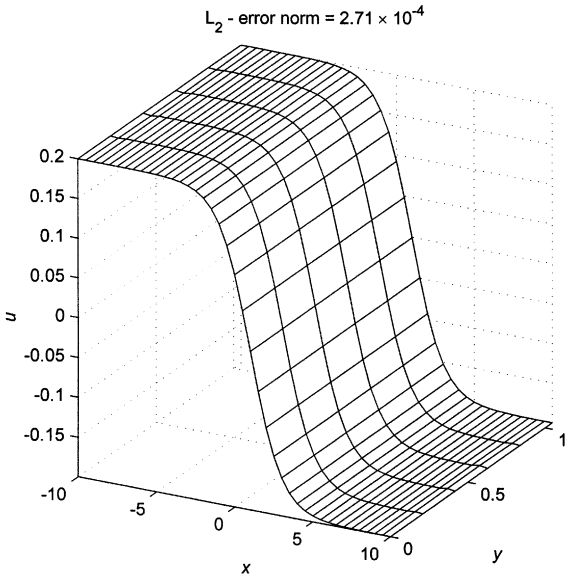


Fig. 10. The solution profile of $u$ computed under $\Delta x = 0.5$ and $\Delta y = \pi/15$.

Our calculation starts from $t = 0.25$ and terminates at $t = 1.25$ for the case with $v = 10^{-2}$.

This problem is chosen to show that the proposed scheme can provide nonoscillatory solutions even in the vicinity of high-gradient region. As is expected, the solution shown in Fig. 11 is nonoscillatory over the entire domain since all chosen grids fall within the monotonic range. For completeness, we also conducted rate of convergence tests from solutions computed at four arbitrarily chosen times $t = 0.997$, 0.998, 0.999 and 1.000. In this rate of convergence test, solutions were obtained at $\Delta t = 10^{-3}$ and $\Delta x = \Delta y = \frac{1}{130}, \frac{1}{135}, \frac{1}{140},$

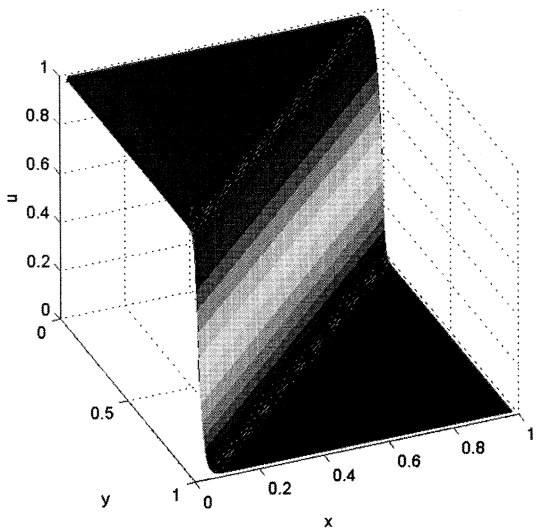


Fig. 11. The nonoscillatory solution profile $u(x, y, 1)$ computed at $\Delta x = \Delta y = 4 \times 10^{-3}$ and $\Delta t = 10^{-3}$.

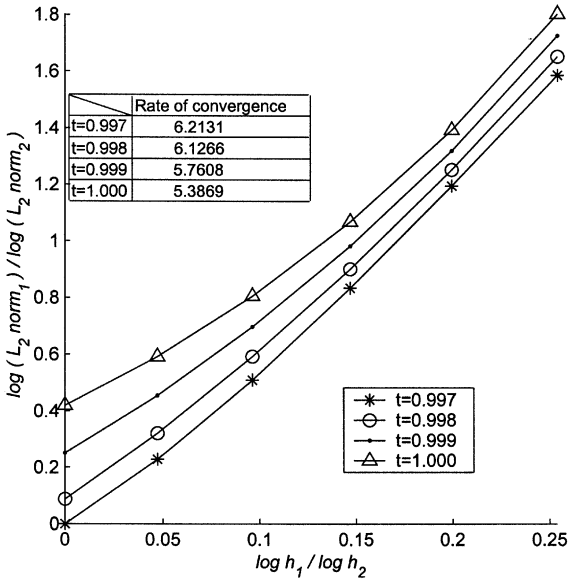


Fig. 12. The computed rates of spatial convergence at four different times.

$\frac{1}{145}$, $\frac{1}{150}$, $\frac{1}{155}$. The spatial rates of convergence shown in Fig. 12 justify the proposed sixth-order accurate finite-difference scheme.

## 6. Concluding remarks

The aim of this numerical study was to circumvent the convective instability problem arising in the nonlinear two-dimensional convection–diffusion transport equation. Our underlying strategy is to exploit the Cole–Hopf mapping to transform the equation under investigation to a Helmholtz equation. The convective instability problem is, thus, completely resolved. In this context, the key to success in predicting the nonlinear convection–diffusion equation lies in the scheme used to solve the Helmholtz equation. For efficiency, we have employed the ADI scheme of Polezhaev. Our main contribution of this study is to develop an unconditionally monotonic sixth-order one-dimensional Helmholtz scheme in a stencil involving only three points. Use of this scheme enables us to effectively obtain the convection–diffusion solution at much less computational cost. Full assessment of the proposed scheme required rigorous testing of the numerical method. For this reason, we considered problems amenable to exact solutions. The computed $L_2$-error norms and their resulting rates of convergence validate the appropriateness of the two-step finite-difference advection–diffusion scheme. For the sake of completeness, computations have been performed to resolve the high-gradient profile. Good ability to capture the sharply varying profile has been demonstrated.

## Acknowledgements

The authors would like to acknowledge the financial support provided by the National Science Council of the Republic of China under grant NSC 88-2611-E-002-025. Also, we like to express thanks to the reviewer who provided useful references about the Helmholtz schemes.

## Appendix A

Consider here the one-dimensional viscous Burgers equation

$$\frac{\partial u}{\partial t} + u\frac{\partial u}{\partial x} - k\frac{\partial^2 u}{\partial x^2} = F. \tag{A.1}$$

For simplicity of presentation, constant diffusivity $k$ is assumed. By employing the Cole–Hopf transformation given below

$$u = -2k\frac{\partial \ln \varphi}{\partial x} = -2k\frac{1}{\varphi}\frac{\partial \varphi}{\partial x}, \tag{A.2}$$

one can easily derive

$$\frac{\partial u}{\partial t} = -2k\frac{\partial\left(\frac{1}{\varphi}\frac{\partial \varphi}{\partial t}\right)}{\partial x}. \tag{A.3}$$

$$\frac{\partial u}{\partial x} = -\frac{2k}{\varphi^2}\left[-\left(\frac{\partial \varphi}{\partial x}\right)^2 + \varphi\frac{\partial^2 \varphi}{\partial x^2}\right], \tag{A.4}$$

$$\frac{\partial^2 u}{\partial x^2} = -\frac{2k}{\varphi^2}\left(-\frac{\partial \varphi}{\partial x}\frac{\partial^2 \varphi}{\partial x^2} + \varphi\frac{\partial^3 \varphi}{\partial x^3}\right) + \frac{4k}{\varphi^3}\frac{\partial \varphi}{\partial x}\left[-\left(\frac{\partial \varphi}{\partial x}\right)^2 + \varphi\frac{\partial^2 \varphi}{\partial x^2}\right]. \tag{A.5}$$

Substitution of Eqs. (A.3)–(A.5) into Eq. (A.1) yields

$$-2k\frac{\partial\left(\frac{1}{\varphi}\frac{\partial \varphi}{\partial t}\right)}{\partial x} + 2k^2\frac{\partial\left(\frac{1}{\varphi}\frac{\partial^2 \varphi}{\partial x^2}\right)}{\partial x} = F. \tag{A.6}$$

Upon integration of the above equation with respect to $x$, we can have

$$\frac{\partial \varphi}{\partial t} = k\frac{\partial^2 \varphi}{\partial x^2} + \varphi\left[\int_0^x \frac{F(\xi)}{-2k}\,\mathrm{d}\xi + C(0,t)\right]. \tag{A.7}$$

For eliminating the undetermined $C(0,t)$, we introduce a new variable $\phi = \varphi\exp(-\int C\,\mathrm{d}t)$ to obtain the following heat conduction equation:

$$\frac{\partial \phi}{\partial t} = k\frac{\partial^2 \phi}{\partial x^2} + \phi\left[\int_0^x \frac{F(\xi)}{-2k}\,\mathrm{d}\xi\right]. \tag{A.8}$$

## References

[1] T.J.R. Hughes, A.N. Brooks, A multi-dimensional upwind scheme with no crosswind diffusion, in: T.J.R. Hughes (Ed.), Finite Element Methods for Convection Dominated Flows, AMD, vol. 34, ASME, New York, 1979, pp. 19–35.
[2] J.D. Cole, On a quasi-linear parabolic equation occurring in aerodynamics, Quart. Appl. Math. 9 (1951) 225–236.
[3] E. Hopf, The partial differential equation $u_t + uu_x = \mu u_{xx}$, Comm. Pure Appl. Math. 3 (1950) 201–230.
[4] F. Ihlenburg, I. Babuška, Finite element solution to the Helmholtz equation with high wave number. Part I: the h-version of the FEM, Comput. Math. Appl. 30 (9) (1995) 9–37.
[5] P. Monk, D.Q. Wang, A least-squares method for the Helmholtz equation, Comput. Meth. Appl. Mech. Engrg. 175 (1999) 121–136.

[6] C.I. Goldstein, The weak element method applied to Helmholtz type equations, Appl. Numer. Math. 2 (1986) 409–426.
[7] K.C. Park, J. Jensen, A systematic determination of lumped and improved consistent map matrices for vibration analysis, AIAA paper No. 89–1335, 1989.
[8] I. Harari, T.J.R. Hughes, Galerkin/least-squares finite element methods for the reduced wave equation with non-reflecting boundary conditions in unbounded domains, Comput. Meth. Appl. Mech. Engrg. 98 (1992) 411–454.
[9] L.L. Thompson, P.M. Pinsky, A Galerkin least-squares finite element method for the two-dimensional Helmholtz equation, Int. J. Numer. Meth. Engrg. 38 (1995) 371–397.
[10] T.J.R. Hughes, Multiscale phenomena: Green's functions, the Dirichlet-to-Neumann formulation, subgrid scale models, bubbles and the origins of stabilized methods, Comput. Meth. Appl. Mech. Engrg. 127 (1995) 387–401.
[11] A.A. Oberai, P.M. Pinsky, A multiscale finite element method for the Helmholtz equation, Comput. Meth. Appl. Mech. Engrg. 154 (1998) 281–297.
[12] X. Yu, Finite difference methods for the reduced water wave equation, Comput. Meth. Appl. Engrg. 154 (1998) 265–280.
[13] L. Lapidus, G.F. Pinder, Numerical Solution of Partial Differential Equations in Science and Engineering, Wiley, New York, 1982.
[14] J.B. Rosser, Nine point difference solutions for Poisson equation, Comput. Math. Appl. 1 (1975) 351–360.
[15] X. Yu, Finite analytic method for the mild slope wave equation, J. Engrg. Mech., ASCE 122 (1995) 109–115.
[16] V.I. Polezhaev, Numerical solution of the system of two-dimensional unsteady Navier-Stokes equations for a compressible gas in a closed region, Fluid Dynam. 2 (1967) 70–74.
[17] T.W.H. Sheu, S.K. Wang, R.K. Lin, An implicit scheme for solving the convection–diffusion-reaction equation in two dimensions, J. Comput. Phys. 164 (2000) 123–142.
[18] R.F. Warming, B.J. Hyette, The modified equation approach to the stability and accuracy analysis of finite-difference methods, J. Comput. Phys. 14 (1974) 159–179.
[19] L.H. Thomas, Elliptic problems in linear difference equations over a network, Watson Sci. Comput. Lab. Rept., Columbia University, New York, 1949.
[20] R.D. Richtmyer, K.W. Morton, Difference Methods for Initial-Value Problems, Interscience, New York, 1967.
[21] T. Meis, U. Marcowitz, Numerical Solution of Partial Differential Equations, Applied Mathematical Science Series, vol. 32, Springer, Berlin, 1981.
[22] T. Ikeda, Maximal Principle in Finite Element Models for Convection–Diffusion Phenomena, Numerical and Applied Analysis, vol. 4, North-Holland Kinokuniya, Amsterdam, Tokyo, 1983.
[23] E.R. Benton, G.W. Platyman, A table of solutions of the one-dimensional Burgers equation, Quart. Appl. Math. (1972) 195–212.
[24] C.A.J. Fletcher, Generating exact solutions of the two-dimensional Burger's equations, Int. J. Numer. Meth. Fluids 3 (1983) 213–216.